# Proton SEU Cross Sections Derived from Heavy-Ion Test Data

Larry D. Edmonds

***Abstract*—Many papers have presented models for estimating proton single event upset (SEU) cross sections from heavy-ion test data, but all rigorous treatments to date are based on the sensitive volume (SV) model for charge collection. Computer simulations have already shown that, excluding devices utilizing physical boundaries for isolation, there is no well-defined SV. A more versatile description of charge collection, which includes the SV model as a special case, utilizes a charge-collection efficiency function that measures the effect that the location of ionization has on collected charge. This paper presents the first rigorous analysis that uses a generic charge-collection efficiency function to relate proton to heavy-ion cross sections. The most practical result is an upper bound for proton SEU or single event latchup (SEL) cross sections, which requires no information about the charge-collection efficiency function, except that it exists. In addition, some models previously presented by others are reproduced (or, in one case, extended) by applying the general theory to special cases. The similarities and differences between a variety of models become clear when the models are recognized to be special cases or variations of this general theory.**

***Index Terms*—Charge-collection depth, charge-collection efficiency, effective flux, proton SEU cross section, SEU, single event upset.**

## I. Introduction

MANY semiconductor devices flown in space are exposed to both heavy ions from galactic cosmic rays (in addition to other possible sources) and a large proton flux from solar events and/or a planetary radiation belt. Regarding single event effects (SEE), the most important types of reactions induced in a device can be different for the two particle types (direct ionization from heavy ions versus the creation of reaction products by protons via nuclear reactions, with the reaction products producing the ionization). Therefore, the most reliable SEE rate calculations utilize experimentally measured device proton cross sections for proton SEE rates, and utilize experimentally measured heavy-ion cross sections for heavy-ion SEE rates. The use of proton data to estimate heavy-ion rates is not widely accepted by the community at present, so many investigators consider heavy-ion tests to be essential for devices that will be exposed to heavy ions. Therefore, a very common situation in practice is that in which a device has been tested with heavy ions but not yet tested with protons. A proton test is an additional expense, so there is a motivation to derive models that predict proton cross sections from heavy-ion test data. This is the subject of the present paper. The analysis is intended for a certain class of SEE in which the physical postulates in Section II are believed to be adequate approximations. Single event upset (SEU) is the prototype assumed in most of the discussions, but the analysis is expected to also apply to single event latchup (SEL). The results derived here are limited to those cases in which direct ionization from protons is not important, so the proton cross section is entirely due to reaction products created by the protons.

Many papers have derived relationships between proton and heavy-ion SEU susceptibility (a good overview of some of the work done prior to 1996 was given by Petersen [1]). However, all rigorous treatments (i.e., the physical postulates are precisely stated, and rigorous analysis is applied to the postulates, e.g., in [2]) to date use the sensitive volume (SV) model as the physical postulate. This model states that the portion of the charge liberated by an ionizing particle that contributes to SEU is the charge liberated within some definite volume within the device. Charge liberated outside the volume is assumed to make no contribution. However, computer simulations show that, excluding devices utilizing physical boundaries for isolation, there is no such volume. Instead, charge collected at a device node changes continuously as the source of ionization (e.g., an ion track) is moved. A more realistic description of charge collection recognizes that charge liberated at any location (within limits established by physical boundaries) makes some contribution to collected charge, but the amount depends on the source location. A physical postulate that is more versatile than the SV model (but includes the SV model as a special case) is that there is a charge-collection efficiency function (a function of the spatial coordinates within a device) that measures the effect of source location on collected charge. The analysis given here is the first rigorous analysis that explicitly includes a charge-collection efficiency function to derive a correlation between heavy-ion and proton SEU or SEL cross sections. A charge-collection efficiency function was theoretically calculated for the special case of total (integrated in time from zero to infinity) charge collection by diffusion [3], but the present paper considers a more generic function, which is any function that adequately satisfies the first postulate in the next section.

The analysis leads to several conclusions. The conclusion having the most practical applications (because it does not require information that is not available) is an upper bound for proton cross sections. Additional conclusions are equalities (instead of inequalities or bounds) derived for each of several special cases. These additional conclusions may become useful if

Manuscript received January 31, 2000; revised May 1, 2000 and June 19, 2000. The research in this paper was carried out by the Jet Propulsion Laboratory, California Institute of Technology, under Contract with the National Aeronautics and Space Administration, Code AE, under the NASA Microelectronics Space Radiation Effects Program (MSREP).

The author is with the Jet Propulsion Laboratory, California Institute of Technology, Pasadena, CA 91109-8099 USA.

Publisher Item Identifier S 0018-9499(00)07569-9.

future work finds ways to obtain the required information, but another motivation for presenting them is academic curiosity. It is interesting to see the similarities and differences between various cases. It is also interesting to compare these conclusions to results previously derived by other investigators.

In spite of limitations of the SV model, nearly all of the numerous published papers that predict proton cross sections from heavy-ion data report good agreement between measured proton cross sections and model predictions. However, previous results generally contain adjustable parameters selected for a good track record, in the sense of producing agreement for the majority of the cases in which comparisons were made between measurement and predictions. Even after a good track record has been established, there is still some uncertainty as to whether a new case of interest will conform to the same pattern. This uncertainty is a risk to a flight project that is relying on model predictions for a particular device that has not been tested with protons. The upper bound presented in Section III contains no arbitrary or adjustable parameters, hence there is no artificial way to obtain a good track record. A disadvantage is that the upper bound can sometimes be excessively conservative, particularly for devices that are completely immune to protons. The only required input information is heavy-ion test data (from long-range, normal-incident ions), which is not enough information to determine proton cross sections, so the upper bound is a more accurate proton cross section estimate for some devices than for others. The upper bound is the proton cross section for the worst possible device (i.e., having the greatest possible proton susceptibility) consistent with the heavy-ion test data. However, it will be seen in Section VI that this "worst" device is not always a rare or hypothetical case. It is fairly common for real devices that are susceptible to protons to be nearly this bad, in the sense that the proton cross sections are within a factor of three of this upper bound.

## II. Physical Postulates

### A. The First Postulate

The first physical postulate assumes that for each point $\boldsymbol{x}$ in a device, there is a weighting function $\Omega(\boldsymbol{x})$ which measures the relative importance of an increment of charge (e.g., a piece of an ion track) liberated at the point $\boldsymbol{x}$, compared to the same amount of charge liberated at other locations. To be more specific, suppose two points in the device $\boldsymbol{x}_1$ and $\boldsymbol{x}_2$ satisfy $\Omega(\boldsymbol{x}_1) = 2\Omega(\boldsymbol{x}_2)$. Then a given amount of charge liberated near the point $\boldsymbol{x}_1$ will produce the same device response as twice this charge liberated near the point $\boldsymbol{x}_2$. The precise and complete statement of the first postulate is that there exists a function $\Omega$ and a constant $Q_c$ (a property of the device) such that

$$SEE\ occurs\ if\ and\ only\ if \quad \int \rho(\vec{x})\Omega(\vec{x})d^3x > Q_c \qquad (1)$$

where $\rho$ is the excess charge density (charge per unit volume) liberated by a particle hit, and the volume integral integrates over the entire device. For SEU, the relevant physical quantity is charge collected at a device node. In this case, $Q_c$ is the critical charge and $\Omega$ can be called a charge-collection efficiency function. For the special case of the SV model, $\Omega$ equals 1 inside the SV and zero outside. Note that if the relevant physical quantity is charge collected over a finite time period associated with some device time constant, then $Q_c$ is the critical value of charge collected over this time period, and $\Omega$ is the weighting function for this quantity. The first postulate is quite general. For example, $Q_c$ could be a time integral of the product of some current (possibly at a device contact, but not necessarily), multiplied by some coefficient that favors current at early times more than current at later times (with "early" and "late" defined by some device time constant). Whatever the physical quantity is that $Q_c$ represents, $\Omega$ is the weighting function for that quantity. The upper bound estimate given in Section III does not require that we even know what kind of physical quantity (e.g., charge collected at a device contact, or something else) that $Q_c$ and $\Omega$ refer to. The only requirement is that some constant $Q_c$ and some corresponding function $\Omega$ satisfying (1) *exist* (we do not have to know what they are). Because of this generality, the theory is expected to apply to SEL as well as to SEU. However, in order to use familiar terminology, the prototype assumed for most discussions is SEU. We will call $Q_c$ the critical charge, and we will call $\Omega$ the charge-collection efficiency function.

A property of the first postulate that may appear to be a severe limitation is that it suggests a certain kind of linearity which will be called the "additive property." For conceptual clarity, assume that the relevant physical quantity is collected charge at some device contact. The additive property is defined to mean that the collected charge from an ion track is the sum of contributions from track sections (with the track partitioned into sections in any arbitrary way), with the contribution from each section calculated with only that section present (all other sections are removed from the device). This is a sufficient condition for the first postulate to apply, but fortunately it is not a necessary condition (as argued later). This is fortunate because the additive property is frequently violated. An example of a violation, in which a track can be less than the sum of its parts, is provided by a DRAM hit by an "overkill" heavy ion (the LET is much larger than needed to cause an SEU for the ion hit location). A DRAM storage capacitor can only collect a finite amount of charge before an associated p–n junction becomes forward biased and charge collection stops. A small track section, taken by itself with all other sections removed from the device, will not see this effect, while an entire overkill track will. The charge collected from the entire track will be less than the sum of contributions when each contribution is from one section without the others present in the device.

An example in which a track is greater than the sum of its parts is charge collection under high-carrier-density conditions. Funneling (enhanced voltage drops across quasi-neutral regions) is a response to, and an indicator of, such conditions (but it is a more dramatic indicator for $n^+$–p junctions than for $p^+$–n junctions) [4], [5]. A small track section taken by itself may not induce such conditions while the entire track does.

Fortunately, two properties taken together help the first postulate to remain valid in spite of violations of the additive property. The first property, which will be called the "JBA property" states that the physical interactions relevant to SEU cross sections are those interactions applicable to particle hits that are just

barely able (JBA) to cause an upset. The relevant interactions for a given ion are those applicable to ion hits at the perimeter of the cross section for that ion. If we assume (right or wrong) that the same physics applies to hits at other locations, the assumed physics may or may not correctly describe charge collection from those other hit locations, but will still correctly predict the SEU cross section. In particular, physical interactions produced by overkill hits are not always relevant (e.g., the above DRAM example). The second property, which will be called the "$Q$-flexibility property" states that the physical quantity (call it $Q$) that $\Omega$ refers to need not be the actual collected charge for all ion hits, as long as it equals (or is any strictly increasing function of, for still more generality) the actual collected charge for JBA hits. If there exists a physical quantity $Q$ having this property and also having the additive property (we do not have to know what $Q$ is, as long as it exists), the first postulate is valid.

For illustration, consider a device (hypothetical if not real) in which a particular approximation explained below applies to charge collection under high-density conditions. This approximation ignores nonlinearities (produced by depletion region boundary motion as a collapsed depletion region expands to its original size [4], [5]) when comparing different high-density conditions, but there is still a nonlinearity associated with the transition between low- and high-density conditions. For low-density conditions, the current collected at a reverse-biased depletion region is the minority-carrier diffusion current calculated from the minority-carrier diffusion equation. For sufficiently global high-density conditions, the approximation is that the current is twice the minority-carrier diffusion current calculated from the ambipolar diffusion equation [4], [5] (incidentally, funneling in this approximation is a response to the current rather than a cause of current in the sense that the potential distribution becomes what is needed to produce the drift currents needed to make the total current be as stated [4], [5]). The actual collected charge does not have the additive property if the entire ion track creates sufficiently global high-density conditions while a small track section alone would not. A way around this problem is to let $Q$ be twice the charge from the minority-carrier diffusion current calculated from the ambipolar diffusion equation. This does have the additive property, so there is an $\Omega$ corresponding to $Q$. If it is also true (a big "if," but assume this for illustration) that all JBA hits produce sufficiently global high-density conditions, then $Q$ equals the actual collected charge for JBA hits, so $Q$ has a critical value and the first physical postulate is valid. The existence of an $\Omega$ satisfying (1) was demonstrated for this hypothetical example by constructing it. Even if we did not know how to construct it, the first physical postulate would still apply (although we may not know it) because the only requirement is that such an $\Omega$ exists (we do not have to know what it is).

Because the above illustration contains some simplifying assumptions, it does not provide a convincing argument that the first physical postulate is always valid (it probably isn't). The intention of this example is merely to argue that the postulate has broader applicability than we would expect if we did not consider the JBA property and the $Q$-flexibility property. Also, the first postulate is more versatile than the SV model, while including this model as a special case. Therefore, even when invalid, the first postulate still approximates reality at least as well as the SV model.

### *B. The Second Postulate*

The second postulate is probably the weakest part of the analysis, and future work may find ways to improve upon this. This postulate is presently needed to simplify the analysis. This postulate assumes that reaction products created by protons have short enough ranges so that $\Omega$ can be approximated as a constant over the reaction product trajectory.

The second postulate has one tendency to produce conservative proton cross section estimates. The worst possible proton reaction allowed by the second postulate is that in which all charge liberated by the reaction products is liberated at a point where $\Omega$ is maximum, i.e., all liberated charge is collected with the maximum efficiency. In reality, if $\Omega$ varies considerably over a reaction product trajectory, then contributions to the liberated charge from different source locations cannot all be collected with the maximum efficiency. Unfortunately, there is another tendency to underestimate proton cross sections. The explanation is simplest for the SV model, so we assume that this model applies for the purpose of illustration. The second postulate does not recognize reactions outside the SV that send reaction products into the SV. In reality this can occur, so the actual proton SEU cross section can include some events in which reactions occur outside the SV, while the calculated cross section excludes such events.

The second postulate is a crude approximation for a real device, but it may not be as bad as the SV model would indicate. To discuss this, we first discuss two types of depths in a device. The most familiar of the two depths is the *charge-collection* depth, defined to be collected charge from a long- (effectively infinite) range normal-incident ion, divided by the charge per unit length liberated along the ion track. The charge-collection depth defined this way is a variable, i.e., a function of the lateral coordinates describing the ion hit location. This was noted by Petersen [6] and later by Barak *et al.* [7] when discussing the cross section associated with the charge-collection depth exceeding a specified value. Petersen has also used other terminology, a charge-collection gain [8], following Massengill *et al.*who reported that some devices exhibit a parasitic bipolar gain that varies as ion hit location is varied [9]. The first physical postulate stated in the previous subsection implies that the charge-collection depth at a given lateral location is the integral of $\Omega$ along a perpendicular line through the device at that lateral location. To simplify this discussion, we are assuming that we do not have to utilize the $Q$-flexibility property, so $\Omega$ refers to actual collected charge (otherwise we would have to refer to $Q$ instead of collected charge). Another depth, the *contributing* depth, is the depth at which $\Omega$ is small enough to be neglected at greater depths. It is only for the SV model that the charge-collection depth and contributing depth are equal. More generally (assuming that $\Omega$ does not exceed 1 anywhere in the device), the contributing depth is larger than the charge-collection depth.

The second physical postulate requires that reaction product ranges (at least for those reaction products that are most important to the device proton cross section) be less than the con-

tributing depth, but this can be more lenient than requiring the ranges to be less than the charge-collection depth. For a hypothetical illustration, suppose that at some lateral location we have $\Omega = 0.1$ within a 10 $\mu$m depth, and $\Omega = 0$ below this depth. The charge-collection depth at this lateral location is only 1 $\mu$m, but the contributing depth is 10 $\mu$m, and the second postulate provides a fairly good approximation when the reaction product ranges are only a few microns. This hypothetical example is probably not very typical, so it does not furnish a convincing argument that the second postulate is a good approximation. The approximation may still be crude, and improving upon this might be a worthwhile objective. The intention of this example is merely to argue that the approximation might be a little better than the SV model would suggest.

## III. An Upper Bound for Proton SEU Cross Sections

It is easy to show that the postulates in Section II imply that the SEU proton cross section $\sigma_{pr}(E)$, for protons having energy $E$, can be expressed as

$$\sigma_{pr}(E) = n \int \alpha\left(E, \frac{Q_c}{\Omega(\vec{x})}\right) d^3x \tag{2}$$

where $n$ is the density of targets (number of silicon atoms per unit volume) and $\alpha(E, Q)$ is the per target cross section for a proton having energy $E$ to produce a reaction that liberates a charge exceeding $Q$. Note that the integrand in (2) is zero at any location where $\Omega = 0$, so the volume integral in (2) can be taken to be over the entire device (in fact, it can be over all space). It is shown in the appendix that the first postulate implies that the cross section $\sigma_{hi}(L)$, for long-range heavy ions having LET $L$, satisfies

$$\int_0^\infty \frac{1}{L} \frac{d\sigma_{hi}(L)}{dL} dL = \frac{a}{Q_c} \int \Omega(\vec{x})\, d^3x \tag{3}$$

where

$$a = 1.04 \times 10^{-10} \frac{\text{coul}}{\text{cm}} [\text{MeV-cm}^2/\text{mg}]^{-1}$$

is a unit conversion factor for converting LET into liberated charge per unit length along the ion track.

Now define $\beta(E)$ by

$$\beta(E) \equiv \max_Q [Qn\alpha(E, Q)]. \tag{4}$$

Note that (4) implies

$$Qn\alpha(E, Q) \le \beta(E)$$

or

$$n\alpha(E, Q) \le \frac{\beta(E)}{Q}$$

so (2) gives

$$\sigma_{pr}(E) \le \frac{\beta(E)}{Q_c} \int \Omega(\vec{x})\, d^3x$$

and using (3) produces the upper bound

$$\sigma_{pr}(E) \le \frac{\beta(E)}{a} \int_0^\infty \frac{1}{L} \frac{d\sigma_{hi}(L)}{dL} dL. \tag{5}$$

## IV. Evaluation of $\beta$

To calculate $\beta$ from (4), we need to evaluate $n\alpha$. The $n\alpha(E, Q)$ used here is the same as the BGR($E$, $E_r$) function used by Normand ([10, Fig. 1]), but with a unit conversion applied so that $n\alpha(E, Q)$ is expressed as a function of liberated charge $Q$ instead of the energy $E_r$ deposited by the reaction products. Note that these data apply to neutrons, which is a good approximation for protons only at the larger values of $E$ (>100 MeV). This should be adequate for practical applications, because the proton saturation cross section (i.e., large $E$ cross section) is the most important parameter for proton-induced SEU rates in typical space environments. This is because a typical proton environment shielded by typical spacecraft shielding is such that most protons having energies large enough to create SEUs, also have energies large enough for the cross section to be roughly equal to the saturation cross section. Therefore, the shape of the $\sigma_{pr}(E)$ versus $E$ curve at small $E$ is only of secondary importance for SEU rate calculations. Also, Barak *et al.* provided an efficiency factor that can be used for refining SEU rate estimates derived from the saturation cross section ([11, Table I]).

A fairly good fit to the data when $E \ge 50$ MeV has the form

$$n\alpha(E, Q) = A(E)e^{-B(E)Q} \tag{6}$$

which gives

$$\beta(E) = \frac{A(E)}{B(E)e}$$

where $A$, $B$, and $\beta$ are given in Table I.

All numerical results given later in this paper apply to 200 MeV. Readers interested in lower energies (which are particularly important when neutrons are a concern) should keep in touch with ongoing research in order to use the most up-to-date $n\alpha$. There has already been a recent refinement for incident energies up to 150 MeV (for both neutrons and protons) [12] not included in Table I. The equations derived in this paper are sufficiently generic so that readers can use the $n\alpha$ of their choice.

## V. Numerical Algorithms

The upper bound proton cross section is given by (5). There are several ways to evaluate the integral in (5). One way is a numerical integration. Another way applies to those cases (which are common but not universal) in which the heavy-ion cross section can be adequately fit by an analytic function having a known integral. A third method is also a numerical integration, but it utilizes an existing computer code that calculates heavy-ion SEU rates in a user-supplied environment. The second two methods are discussed separately in the first two subsections. Other considerations, regarding the amount and type of data to be used, are discussed in the last two subsections.

TABLE I
FITTING PARAMETERS $A$ AND $B$ FOR $n\alpha$, AND THE IMPLIED $\beta$

| E (MeV) | A(E) (1/cm) | B(E) (1/pC) | β(E) (coul-μm²/cm³) |
|---|---|---|---|
| 50 | 0.030 | 23.099 | $4.78 \times 10^{-8}$ |
| 100 | 0.022 | 14.433 | $5.61 \times 10^{-8}$ |
| 200 | 0.020 | 9.935 | $7.41 \times 10^{-8}$ |

### A. Evaluation via an Exponential Fit

A simple function that frequently (not always) produces a good fit to heavy-ion SEU or SEL cross section data is given by

$$\sigma_{hi}(L) = \sigma_0 \exp\left(-\frac{L_{1/e}}{L}\right) \tag{7}$$

where $\sigma_0$ (a constant) is the saturation cross section, and $L_{1/e}$ (a constant) is the LET value at which the cross section is $1/e$ times the saturation cross section. Although (7) was derived from physical analysis [13], it does not apply to all cases. One reason (perhaps not the only reason) is that a sum of functions of the type given by (7) is not another function of the same type, unless $L_{1/e}$ is the same for all terms in the sum. Therefore (7) does not apply to devices containing dissimilar components that contribute to the cross section. However, (7) is worth considering, because it frequently does apply, and a test for determining whether it does apply is very simple. The test plots the cross section against $1/L$ on semi-logarithmic paper (the cross section uses the logarithmic scale), and (subject to qualifications in the next paragraph) we look for a straight line.

Two considerations are relevant when testing the applicability of (7). The first involves cosine-law errors. Heavy-ion tests typically change the tilt angle of the device relative to the ion beam to mimic a change in ion LET, and the data are then converted via an assumed cosine law. The converted data are intended to represent the device susceptibility at normal incidence. However, the cosine-law conversion is only an approximation, and not always a good approximation. An unfortunate property of the popular Weibull function is that it fits a certain class of cosine-law errors (those giving the illusion of a fast approach to saturation) very well. This is unfortunate because cosine-law errors are not always noticed (incidentally, Petersen suggests that a log normal distribution might be better than the Weibull fit [8]). The fit given by (7) generally does not fit cosine-law errors, so preference should be given to data measured at normal incidence when determining whether the fit applies.

The second consideration is that (7) has no threshold LET (the LET at which the cross section is zero). This is not a concern as long as the cross section calculated from (7) is negligibly small at LET less than the experimentally measured threshold LET. The straight line previously discussed often fails to fit the smallest LET (largest 1/LET) data, but this is usually not an important concern.

An example is provided by data obtained by Levinson *et al.* [14] for the HM65162 SRAM produced in 1985 (the year is relevant because there are different versions of the device having different SEL cross sections). Measured heavy-ion cross section data (points), and a fit (curve) obtained from (7) are shown in Fig. 1. The fitting parameters are $\sigma_0 = 0.116$ cm$^2$, $L_{1/e} = 28.3$ MeV-cm$^2$/mg. It is not known which, if any, of the points might contain cosine-law errors (i.e., were measured at angles), so the fit attempted to accommodate all points. The seemingly low cross section at the largest LET data point might be influenced by a recombination loss discussed by Levinson *et al.* [14], so this point was given a low priority when selecting the fit. If this point is meaningful, then the fit overestimates the cross section, but this is okay for an upper bound estimate of $\sigma_{pr}$. Note that the calculated cross section is negligible for LET below that of the lowest LET point, even though (7) has no threshold LET.

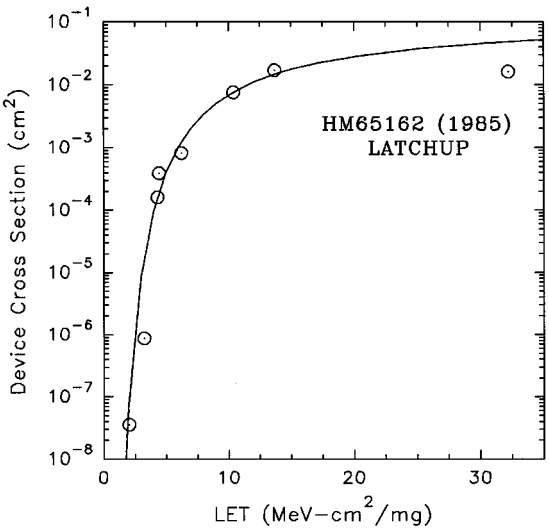


Fig. 1. Heavy-ion SEL cross section for the HM65162 SRAM produced in 1985. Data (points) are from Levinson *et al.* [14]. The curve is from (7) using $\sigma_0 = 0.116$ cm$^2$, $L_{1/e} = 28.3$ MeV-cm$^2$/mg.

For those devices such the (7) provides an adequate approximation, the integral in (5) can be evaluated, and the result is

$$\sigma_{pr}(E) \leq \frac{\beta(E)}{a}\,\frac{\sigma_0}{L_{1/e}}\ (equivalent\ to\ (5)\ when\ (7)\ applies). \tag{8}$$

### B. Evaluation via a Heavy-Ion Rate Calculation

This method performs a numerical integration by using an existing computer code that calculates heavy-ion SEU rates in a user-supplied environment. The physics assumed by the code must be consistent with the first postulate in Section II, but this includes the SV model, which is used in the standard codes. This is a convenient method for individuals accustomed to calculating heavy-ion SEU rates, because no programming is required, and routine calculations can be used.

Most of the discussion below justifies the conclusion at the end. Readers willing to believe the conclusion without seeing the justifications can skip to the last paragraph in this subsection, which describes the algorithm.

To derive the algorithm, note that (3) applies not only to cross sections measured at normal incidence, but also to cross sections measured at any angle, if $\sigma_{hi}$ is interpreted as the directional

cross section. Therefore

$$\left[\int_0^\infty \frac{1}{L}\frac{d\sigma_{hi}(L)}{dL}\,dL\right]_{normal\ incidence} = \left[\int_0^\infty \frac{1}{L}\frac{d\sigma_{hi}(L)}{dL}\,dL\right]_{any\ angle}.$$

The solid angle integral of the above equation produces a heavy-ion SEU rate in an isotropic environment (with the integral LET flux proportional to $1/L$) on the right side. The result is

$$\frac{1}{a}\int_0^\infty \frac{1}{L}\frac{d\sigma_{hi}(L)}{dL}\,dL = r^*\left[\text{day-cm}^2\frac{\text{cm}^3}{\text{coul-}\mu\text{m}^2}\right] \quad (9)$$

where $r^*$ is defined by

$r* \equiv$ Heavy-ion rate for a device having a normal-incident cross section $\sigma_{hi}$ and produced by an integral LET flux $H^*$ given by $H^*(L) = (0.8856/\text{m}^2\text{-sec-ster})(\text{MeV-cm}^2/\text{mg})/L$.

The constant in the flux $H^*$ was selected so that inconvenient constants do not appear in (9). The flux $H^*$ will be called the hypothetical $1/L$ flux. Substituting (9) into (5) gives

$$\sigma_{pr}\#(E) \le \beta\#(E)r^*\#\ (equivalent\ to\ (5)) \quad (10)$$

where the quantities in (10) are the dimensionless numbers defined by

$$\sigma_{pr}\#(E) \equiv \sigma_{pr}(E)/\text{cm}^2$$
$$\beta\#(E) \equiv \beta(E)/[\text{coul-}\mu\text{m}^2/\text{cm}^3]$$
$$r^*\# \equiv r^*/[1/day].$$

In other words, $\sigma_{pr}\#(E)$ is the numerical part of $\sigma_{pr}(E)$ when expressed in the units of $\text{cm}^2$. Analogous statements apply to the other quantities.

Note that $r^*$ would not be well defined if the flux was other than the hypothetical $1/L$ flux, because a normal-incident cross section would not otherwise uniquely determine the heavy-ion SEU rate. Different devices can have the same normal-incident data but different directional cross sections at other angles. This difference will produce different SEU rates in most heavy-ion environments. However, (9) implies that, for this special and hypothetical heavy-ion environment, different devices having the same normal-incident data also have the same heavy-ion SEU rate, even though they may have different directional cross sections at other angles.

Readers that would like to see a demonstration of the above assertion can do so by using a standard computer code that calculates the heavy-ion SEU rate for the traditional rectangular parallelepiped (RPP) shaped SV. All RPPs being compared are given the same upper surface areas and threshold LETs, so that they have the same normal-incident cross section curve, but they are given different thicknesses (with correspondingly different critical charges so that the threshold LETs are the same). In most environments, the calculated rate for each RPP will depend on the RPP thickness. However, for the hypothetical $1/L$ flux, the same rate will be calculated for all choices of the RPP thickness (except for numerical errors, e.g., associated with data interpolation/extrapolation and/or approximations for chord-length distribution functions).

Any computer code consistent with the first postulate in Section II should calculate the same value for $r^*$. Note, however, that the conventional model used for smooth device cross section curves is the integral RPP (IRPP) model, which regards a device as a collection of RPPs, that may have different critical charges (at least this is the original statement of the RPP model [15]). This model does not satisfy the first postulate in Section II, because different values of $Q_c$ are associated with different RPPs. However, each RPP satisfies the postulate, so (5), (9), and (10) apply to the individual RPPs. Summing these results over the RPPs produces the same results (5), (9), and (10) but with the cross sections interpreted as device cross sections. We can therefore use these results together with the traditional IRPP method for calculating $r^*$ (the RPP thickness is arbitrary because the same $r^*$ is calculated for any thickness).

Most existing computer codes that can be used to calculate $r^*$ accept the environment in the form of a table of heavy-ion flux versus LET. If the code allows the user to select the LET values appearing in the table, we must consider both numerical errors from coarseness of the tabulation, and whether the code will have to extrapolate outside the range of the table (keeping in mind that thin RPPs require the flux to be evaluated at LETs much less than the threshold LET). Based on these considerations, a suggested tabulation is

$$L_i\# = 10^{((i/25)-3)}, \quad H_i^*\# = \frac{0.8856}{L_i\#} \quad \text{for } i = 0, 1, \cdots, 175 \quad (11a)$$

where

$$L_i\# \equiv L_i/[\text{MeV-cm}^2/\text{mg}]$$
$$H_i^*\# \equiv H_i^*/[1/\text{m}^2\text{-sec-ster}].$$

If the computer code accepts the environment in the form of a differential (in LET) flux $h^*$ instead of an integral flux $H^*$, a suggested tabulation is

$$L_i\# = 10^{((i/25)-3)}, \quad h_i^*\# = \frac{0.8856}{L_i\#^2} \quad \text{for } i = 0, 1, \cdots, 175 \quad (11b)$$

where

$$h_i^*\# \equiv h_i^*/[(1/\text{m}^2\text{-sec-ster})/(\text{MeV-cm}^2/\text{mg})].$$

The numerical algorithm for calculating an upper bound for the proton cross section via the rate calculation method is summarized as follows. A standard computer code designed to calculate heavy-ion SEU rates in a user supplied isotropic environment is used. The environment given to the code is either the integral flux $H^*$ or the differential flux $h^*$ (as dictated by the computer code), which can be tabulated as indicated in (11a) and (11b). The code is also given the device heavy-ion cross section data, and the code calculates the heavy-ion SEU rate $r^*$. If the code uses the IRPP method, the RPP thickness is arbitrary

(the same $r^*$ will be calculated from any thickness) as long as the thickness is not extreme enough to create large numerical errors. The upper bound estimate is then obtained from (10), with $\beta$ obtained from Table I.

### C. The Relevant LET Range

A property of the integral in (5) that may seem unfortunate is that significant contributions to the integral can come from the high-LET portion of the $\sigma_{hi}$ curve; from LETs larger than we might expect to be relevant to proton cross sections. Three reasons for this are:

1) A conservative property of the second physical postulate (Section II) tends to exaggerate the importance of the high-LET portion of the $\sigma_{hi}$ curve.
2) Intentional conservatism that makes the estimate for $\sigma_{pr}$ an upper bound can sometimes exaggerate the importance of the high-LET portion of the $\sigma_{hi}$ curve.
3) Some contribution to $\sigma_{pr}$ from the higher-LET portions of the $\sigma_{hi}$ curve is real. This was pointed out be Petersen [16]. Furthermore, the experimentally measured $\sigma_{pr}$ can sometimes be under-estimated by not integrating to large enough LET, again indicating that some contribution to $\sigma_{pr}$ from the higher-LET portions of the $\sigma_{hi}$ curve is real.

It is not always clear how much of the high-LET contribution to $\sigma_{pr}$ is an exaggeration and how much of it is real. Therefore, the upper bound estimate for $\sigma_{pr}$ cannot be considered to be a reliable upper bound unless the integration includes all LETs that significantly contribute to the integral in (5). This generally means integrating to near saturation of the $\sigma_{hi}$ curve. One way to do this is to use the exponential fit for $\sigma_{hi}$ together with (8), which includes all contributions from the complete curve. Another way is to use a Weibull fit for $\sigma_{hi}$ together with the rate calculation method. A good computer code that calculates heavy-ion rates from Weibull parameters will include all relevant LETs.

A problem is most likely when no fit is used and many points are read directly from the $\sigma_{hi}$ plot. This is tedious, so it is tempting to exclude the higher-LET points. Devices having threshold LETs greater than 12 MeV-cm$^2$/mg are often assumed to be immune to protons, so it is tempting to ignore the portion of the $\sigma_{hi}$ curve having $L > 12$. An example in which this is inadequate is furnished by the AMD K-5 microprocessor. Heavy-ion SEL data (from internal JPL memos) are plotted in Fig. 2. The two highest points are very crude estimates, because the SEL rate was large enough to overwhelm the instrumentation at these points. The points were not fit, so the curve in the figure is a hand sketch. If the portion of the curve having $L > 12$ is ignored, the upper bound for $\sigma_{pr}$ calculated from (10) for $E = 200$ MeV is only $1.1 \times 10^{-9}$ cm$^2$. The measured value is $5.6 \times 10^{-9}$ cm$^2$, so the intended upper bound actually underestimated the cross section. However, if the entire plotted range of the curve is included, the calculated upper bound becomes $1.9 \times 10^{-8}$ cm$^2$.

### D. MBUs

Devices soft enough to be susceptible to protons are often also susceptible to multiple-bit-upsets (MBUs) from heavy ions

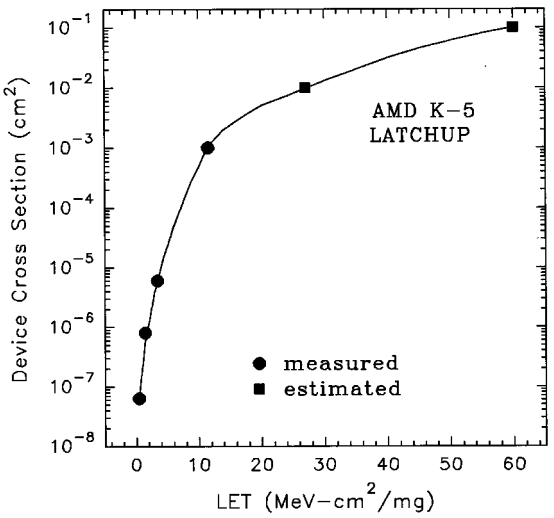


Fig. 2. Heavy-ion SEL cross sections for the AMD K-5 microprocessor. Data (points) are from internal memos, but the two highest points are very crude estimates. The curve is a hand sketch.

(sometimes also protons), i.e., one particle hit upsets several bits or cells. The first physical postulate can explain MBUs more easily than the SV model. An attempt to explain MBU from normal-incident heavy ions via the SV model assumes that SVs for different cells overlap. But this implies that several cells each collect all of the charge liberated in the overlapping region, so this attempted explanation is unrealistic. In contrast, the first postulate easily explains MBU in terms of charge sharing by different cells. Each cell has its own $\Omega$ function, and these functions can overlap, but with each $\Omega$ small enough so that the sum of the $\Omega$s at any given location does not exceed 1. Some fraction of the liberated charge is collected by one cell, and another fraction is collected by another cell. Charge collected by a given cell is well defined in this model for any heavy-ion hit location, even if the ion hits another cell. This makes an individual cell cross section for a given heavy ion well defined, in terms of the hit locations that will upset that cell. Individual cell cross sections increase with increasing ion LET, and can sometimes become large enough to overlap. Hits to overlap regions produce MBUs.

Several types of device cross sections can be defined. One type, called the U-type here (U for upset), is calculated from the total number of upsets observed during an SEU test, while another type, called the G-type here (G for group), counts the number of occurrences of upset groups. An upset group is defined here to be the set of upsets (one or more) produced by the same particle hit. For example, if one particle hit upsets four cells, the U-type cross section counts this as four upsets, while the G-type counts this as one group. The G-type is useful when one upset group is regarded as one device failure, regardless of whether the group contains one or many cell upsets. There are also variations of the G-type, e.g., the G3-type, which counts the number of occurrences of groups containing three upsets. The G-type device cross section is the sum in $n$ of the G$n$-type cross sections, while the U-type is the sum in $n$ of $n$ times the G$n$-type.

Only the U-type device cross section has the property of being the sum of the bit or cell cross sections. The U-type device cross

section can be larger than the area of the entire device, because cell cross sections can overlap to the extent that the sum of these cross sections is larger than the device area. If all cells in the device are identical, the cell (or bit) cross section is the U-type device cross section divided by the number of cells in the device. In contrast, while a G-type device cross section can be numerically divided by the number of bits and reported as a per-bit cross section, it is physically meaningless to associate this with an individual cell.

The upper bound given by (5) was actually derived for an individual cell rather than an entire device. The bound can be applied to devices by summing over cells. If we apply (5) to each cell and sum over cells, we obtain the same result (5), except that the cross sections are now sums of cell cross sections. These sums are U-type device cross sections. Therefore, the U-type $\sigma_{hi}$ can be used in (5) to obtain an upper bound estimate for the U-type $\sigma_{pr}$. It is plausible that the G-type $\sigma_{hi}$ can be used for the G-type $\sigma_{pr}$. The arguments used here neither support nor contradict this assertion. Investigating the validity of this assertion might be a subject for future work. The conclusion that is supported here is that U-types are used to estimate U-types.

DRAMs are especially prone to MBU, and they are also especially prone to cosine-law errors. The U-type device heavy-ion cross sections (and therefore the cell cross sections) for DRAMs are sometimes better described as isotropic than by the cosine law (the G-type may have some other angular dependence, but this is not related in a simple way to the cell cross section). Therefore, data intended to represent the heavy-ion susceptibility of a DRAM at normal incidence should be measured at normal incidence, as opposed to using an assumed cosine-law conversion with data measured at angles.

## VI. Comparisons with Measured Data

Calvel *et al.* [17] and Petersen [18] each compiled a list of devices tested for SEU using both heavy-ions and protons. Weibull parameters for the heavy-ion cross sections were provided for each device, so an upper bound estimate for $\sigma_{pr}$ is easily calculated from (10), using a computer code that calculates heavy-ion SEU rates and that accepts Weibull parameters as input. The calculated and measured saturation proton cross sections are compared in Table II (no distinction is made here between the saturation cross section and the cross section at $E = 200$ MeV). SEU data in the upper block in the table are from Calvel *et al.* [17]. Data from Petersen [18] that are not already in the upper block are in the second block (excluding two devices as discussed at the end of this section). The Weibull parameters are included in the table so that readers possessing a computer code as discussed above can easily reproduce the estimates for $\sigma_{pr}$. SEL data for the last two devices (lower block) in the table were discussed in previous sections. The last column is the calculated $\sigma_{pr}$ divided by the measured $\sigma_{pr}$.

Note that the upper bound is within a factor of three of the measured cross section for most of the SEU cases listed. The SEL entries are consistent with a known trend. Given two devices having the same $\sigma_{hi}$ curve, but one refers to SEU and the other refers to SEL, the proton cross section is usually (perhaps not always) smaller for the SEL case. Therefore the upper bound estimate will often be excessively conservative for SEL (e.g., the HM65162). However, the K-5 shows that there are also cases in which the upper bound is only moderately conservative.

Two devices were omitted from the second block in Table II. One is the AMD version of the 93L422. The upper bound estimate for this device under-estimated the reported proton cross section by a factor of six, and this motivated a search for the original data. This search revealed that the Weibull fit in [18] underestimates the heavy-ion cross section data [19] by a consistent (various LET) factor of either about two or three, depending on which of the two tested devices is selected for comparison. It was also found that scatter in the proton data [20] spans a factor of five, with the most pessimistic data point appearing in the subsequent literature (internal JPL memos commented on large part-to-part variations, and problems with proton-beam control and dosimetry). While these data are adequate for SEU rate estimates, the precision is inadequate for testing or refining theoretical models. Incidentally, this search also revealed considerable part-to-part variations in the Fairchild version of the 93L422 (internal JPL memos), so the slight under-estimation in Table II for this device is not too alarming. The other omitted device is the 2164. The upper bound estimate for this device under-estimated the reported proton cross section by a factor of almost two, and this motivated another search for the original data. It was found that several types of heavy-ion cross sections were measured [2], but the type appearing in the subsequent literature is the G-type discussed in Section V-D. The U-type is about twice the G-type. Use of the G-type may or may not be valid, but it was also found that the proton cross section reported in [18] was more than twice the value reported in [2].

## VII. Equalities for Several Special Cases

This section derives equalities (instead of inequalities or bounds) for several special cases. The results have limited practical applications because they are only useful for SEU or SEL rate calculations if we have information that is rarely available. Future work may find ways to obtain the required information, but another motivation for this section is academic curiosity. It is interesting to see the similarities and differences between various cases. Furthermore, the results derived in this section can be compared to results previously derived by other investigators. This comparison is made in the next section.

### A. Case 1: A Single but Arbitrary SV

The first special case is a single SV having an arbitrary shape. The thickness measured in the vertical direction can vary with the lateral coordinates. This variable thickness accounts for the gradual increase in the normal-incident $\sigma_{hi}(L)$ versus $L$ curve, as previously pointed out by Langworthy [21]. Using $\Omega = 1$ inside the SV and $\Omega = 0$ outside, (2) and (3) reduce to

$$\sigma_{pr}(E) = n\alpha(E, Q_c) \int_{SV} d^3x,$$

$$\int_0^\infty \frac{1}{L} \frac{d\sigma_{hi}(L)}{dL}\, dL = \frac{a}{Q_c} \int_{SV} d^3x$$

TABLE II
COMPARISON BETWEEN PREDICTED AND MEASURES PROTON SATURATION CROSS SECTIONS. DATA IN THE FIRST BLOCK ARE FROM CALVEL *et al.* [17], AND DATA IN THE SECOND BLOCK ARE FROM PETERSON [18]. DEVICES IN THE THIRD BLOCK WERE DISCUSSED IN EARLIER SECTIONS

| Part | Weibull Parameters ($L_0$ and W in MeV-cm$^2$/mg, C in cm$^2$) | | | | Data | Upper Bound | Ratio |
|---|---|---|---|---|---|---|---|
| | $L_0$ | C | W | S | $\sigma_{pr}$(sat.) (cm$^2$) | $\sigma_{pr}$(sat.) (cm$^2$) | |
| SMJ44100 (SEU) | 1.39 | 2.0E0 | 15.0 | 1.21 | 7.00E-7 | 1.9E-6 | 2.7 |
| 62256R (SEU) | 1.60 | 6.4E-1 | 20.0 | 1.65 | 1.47E-7 | 3.8E-7 | 2.6 |
| IBM 16MEG (SEU) | 1.70 | 1.3E-1 | 20.0 | 3.00 | 2.12E-8 | 5.8E-8 | 2.7 |
| MT4C1004C (SEU) | 1.54 | 1.3E0 | 14.5 | 1.45 | 3.94E-7 | 1.0E-6 | 2.5 |
| KM41C4000Z-8 (SEU) | 1.52 | 1.3E0 | 18.0 | 1.45 | 3.27E-7 | 8.9E-7 | 2.7 |
| 01G9274 (SEU) | 1.60 | 9.7E-2 | 28.0 | 3.25 | 4.19E-9 | 3.1E-8 | 7.4 |
| OW 62256 (SEU) | 2.40 | 4.3E-1 | 16.5 | 2.25 | 8.70E-8 | 2.3E-7 | 2.6 |
| MT4C4001 (SEU) | 1.49 | 1.3E0 | 15.0 | 1.21 | 2.94E-7 | 1.2E-6 | 4.1 |
| HM6116 (SEU) | 4.20 | 6.6E-2 | 7.9 | 2.50 | 4.59E-8 | 4.7E-8 | 1.0 |
| 62832H (SEU) | 3.40 | 1.0E-1 | 20.0 | 1.50 | 2.89E-8 | 5.0E-8 | 1.7 |
| 2901B (SEU) | 4.20 | 3.0E-3 | 10.0 | 1.50 | 8.5E-10 | 2.1E-9 | 2.5 |
| TC514100Z-10 (SEU) | 0.86 | 2.1E0 | 18.0 | 1.15 | 1.00E-6 | 2.0E-6 | 2.0 |
| HM 65656 (SEU) | 1.50 | 1.1E-1 | 12.0 | 1.75 | 2.98E-8 | 9.6E-8 | 3.2 |
| MB814100 10PSZ (SEU) | 1.15 | 3.2E0 | 15.0 | 1.35 | 6.90E-7 | 2.9E-6 | 4.2 |
| HYB514100J-10 (SEU) | 0.86 | 2.1E0 | 14.0 | 1.10 | 1.46E-6 | 2.5E-6 | 1.7 |
| LUNA C (SEU) | 3.20 | 1.5E-1 | 14.0 | 3.00 | 2.12E-8 | 8.2E-8 | 3.9 |
| D424100V-80 (SEU) | 0.80 | 1.5E0 | 10.0 | 1.10 | 1.76E-6 | 2.3E-6 | 1.3 |
| HM6516 (SEU) | 5.00 | 3.0E-2 | 14.0 | 1.90 | 2.46E-9 | 1.6E-8 | 6.5 |
| Fairchild 93L422 (bipolar) (SEU per bit) | 0.6 | 2.6E-5 | 4.4 | 0.7 | 1.4E-10 | 9.6E-11 | 0.70 |
| Samsung 16M 3.3V DRAM (SEU per bit) | 0.6 | 9.87E-8 | 16.39 | 1.85 | 3.5E-14 | 7.4E-14 | 2.1 |
| Hitachi 16M 3.3V DRAM (SEU per bit) | 0.5 | 2.27E-8 | 7.9 | 4.11 | 1.6E-14 | 2.4E-14 | 1.5 |
| Micron 16M 3.3V DRAM (SEU per bit) | 0 | 1.92E-8 | 8.98 | 5.37 | 8.0E-15 | 1.9E-14 | 2.3 |
| IBM E 16M 3.3V DRAM (SEU per bit) | -0.4 | 2.6E-9 | 7.89 | 5.39 | 1.7E-15 | 2.8E-15 | 1.6 |
| K-5 (SEL) | NA: See Section V-C | | | | 5.6E-9 | 1.9E-8 | 3.4 |
| HM65162 (1985) (SEL) | NA: See Section V-A | | | | 1.4E-10 | 2.9E-8 | 210 |

which gives

$$\sigma_{pr}(E) = \frac{Q_c n\alpha(E, Q_c)}{a} \int_0^\infty \frac{1}{L} \frac{d\sigma_{hi}(L)}{dL}\, dL. \qquad (12)$$

Note that if it is somehow known that the single SV model does apply to a device, but $Q_c$ is unknown, then the supplementary information (that the single SV model applies) cannot be used to reduce the bound given by (5). Without knowing $Q_c$, the best bound obtainable for (12) is still given by (5). In fact, we see from (12) that the upper bound given by (5) is not overkill, because this limit can be reached by any device adequately described by the single SV model and having a special value for the critical charge. This special value is the maximizing $Q$ in (4). Using the data in Table I, we calculate this maximizing $Q$ (which is $1/B$) to be about 0.1 pC when $E = 200$ MeV.

The derivation of (12) assumed a single SV, but summing cross sections produces the same result for any collection of SVs having identical values for $Q_c$.

The assumption that $\Omega = 1$ inside the SV is appropriate when $Q_c$ is the critical value of the charge liberated within the SV. If the SV is subject to some kind of transistor gain amplification, the charge collected at a device contact could differ from the liberated charge. For example, if an amplification results in the collected charge being twice the liberated charge, and if $Q_c$ refers to the critical value of the collected (or amplified) charge instead of the critical value of the liberated charge, then $\Omega = 2$ inside the SV. A generalization of (12), which allows $\Omega$ to be any positive constant (denoted $\Omega_0$) in the SV is

$$\sigma_{pr}(E) = \frac{1}{a} \frac{Q_c}{\Omega_0} n\alpha\left(E, \frac{Q_c}{\Omega_0}\right) \int_0^\infty \frac{1}{L} \frac{d\sigma_{hi}(L)}{dL}\, dL.$$

### *B. Case 2: A Collection of RPPs Having a Distribution of Critical Charges*

Previous results apply to a device having a single value of $Q_c$. A device containing several components, having different values of $Q_c$, can be treated by simply adding the cross sections for each component. The original postulate behind the IRPP method for calculating heavy-ion rates [15] is that there is a collection of RPP shaped SVs producing a distribution of values of $Q_c$. The gradual increase in the heavy-ion cross section with increasing ion LET is attributed to an increasing number of contributing RPPs with increasing LET. To describe this case, we can use (12) for each RPP [the heavy-ion cross section in (12) becomes a step function when applied to an RPP, allowing the

right side to be expressed without an integral], and sum (or integrate) the individual RPP cross sections to obtain the device cross section. The result need not be listed here because it is identical to the result derived in Case 4 discussed later. The two cases produce the same result because of a mathematical equivalence pointed out in the discussion of Case 4.

### C. Case 3: A Partially Separable $\Omega$

This case applies when $\Omega$ can be adequately approximated by a partially separable function; a function of $z$ alone times a function of $x$ and $y$ alone ($z$ measures depth, and $x$ and $y$ are two lateral coordinates). We write $\Omega$ as

$$\Omega(x, y, z) = f(x, y)g(z) \tag{13}$$

for some functions $f$ and $g$. This equation can be written as

$$\Omega(x, y, z) = \tau(x, y)\frac{g(z)}{I} \tag{14}$$

where the charge-collection depth $\tau$ and the integral $I$ are defined by

$$\tau(x, y) \equiv \int_{-\infty}^{\infty} \Omega(x, y, z)\, dz = f(x, y)I,$$
$$I \equiv \int_{-\infty}^{\infty} g(z)\, dz.$$

Substituting (14) into (2) gives

$$\sigma_{pr}(E) = \int G(E, \tau(x, y))\, dx\, dy$$

where $G$ is defined by

$$G(E, \xi) \equiv n \int_{-\infty}^{\infty} \alpha\left(E, \frac{Q_c I}{\xi g(z)}\right) dz. \tag{15}$$

It is shown in the Appendix that the above equation for $\sigma_{pr}$ can be written as

$$\sigma_{pr}(E) = \int_0^{\infty} G\left(E, \frac{Q_c}{aL}\right) \frac{d\sigma_{hi}(L)}{dL}\, dL. \tag{16}$$

### D. Case 4: Lateral Variation within a Uniform Contributing Depth

This case, which is a further specialization of the previous case, assumes that charge collection is confined to a horizontal layer having a uniform thickness $T$. $\Omega$ is independent of $z$ (but it may still depend on the lateral coordinates) within this layer, and $\Omega = 0$ above or below this layer. This case is obtained from Case 3 by letting $g$ in (13) satisfy $I/g(z) = T$ when $z$ is inside the horizontal layer, and $g(z) = 0$ when $z$ is outside. For this case, (15) reduces to

$$G(E, \xi) = n\alpha\left(E, \frac{Q_c T}{\xi}\right) T$$

and (16) becomes

$$\sigma_{pr}(E) = T \int_0^{\infty} n\alpha(E, aLT) \frac{d\sigma_{hi}(L)}{dL}\, dL. \tag{17}$$

This result also applies to the collection of RPPs (Case 2) with $T$ the RPP thickness, because there is a mathematical equivalence between that case and the present case. The equivalence applies to normal-incident heavy ions [note that unlike the integral in (5) and (12), the integral in (17) is not rotationally invariant, so the heavy-ion data must refer to normal incidence]. The equivalence is due to the fact that (for normal-incident hits) an $\Omega$ that varies with the lateral coordinates combined with a constant $Q_c$ (this case) is equivalent to a $Q_c$ that varies with the lateral coordinates (from one RPP to the next) combined with a constant $\Omega$ (Case 2).

It is interesting that (17) is not equivalent to the result (12) for a single but general SV (Case 1). A comparison between the two equations shows a fundamental difference between a collection of RPPs and a single but general SV (having a variable thickness), even though both cases can produce the same $\sigma_{hi}$ curve. The same $\sigma_{hi}$ curve can lead to different estimates for $\sigma_{pr}$, depending on which model is assumed to apply. A device described by both Case 1 and Case 4 (or Case 2) is characterized by an SV with uniform depth, so the heavy-ion cross section curve is a step function and the two equations, (12) and (17), give the same result. Otherwise, the two equations give different results.

If it is somehow known that Case 2 applies, an estimate for $T$ might be obtained from a method discussed by Petersen [22]. Note however, that while Cases 2 and 4 are indistinguishable in terms of heavy-ion hits at normal incidence, they are distinguishable in terms of the directional dependence of the heavy-ion cross section for hits at angles. Case 2 is equivalent to a modified Case 2 in which the same $Q_c$ is assigned to all RPPs and $\Omega$ is uniform within each RPP, but $\Omega$ is different for different RPPs. However, the original and modified Case 2 regard all RPPs as spatially isolated. To obtain Case 4, we must move the RPPs in the modified Case 2 next to each other and add collected charges from all, so that a hit at an angle can simultaneously intersect several RPPs, with each adding a contribution to the collected charge. The heavy-ion cross section will have a different directional dependence for isolated RPPs (Case 2) than for adjacent RPPs (Case 4) that can each contain a section from the same track and contribute to collected charge. Therefore, while Petersen's method applies to Case 2, it has not yet been shown to be valid for Case 4 (incidentally, these considerations suggest that Petersen may have overlooked some complications when arguing that the traditional IRPP heavy-ion rate calculation applies to a modified version of the RPP model [8]).

## VIII. Some Recent Work

A number of results relating proton cross sections to heavy-ion cross sections have been presented in the recent literature. One motivation for discussing some of these results here is to acknowledge some of the recent work previously done by others. In particular, the result for Case 2 (Section VII) was previously derived by Normand, as discussed below. Another motivation for discussing these results is that it is interesting to see the similarities and differences between various theories. These similarities and differences become

clear after recognizing that various results are special cases of (and easily reproduced from) the more general theory in the present paper. In particular, it will be seen that a result by Normand and a result by Johnston *et al.*were derived from physically different but mathematically equivalent assumptions (Case 2 versus Case 4 in Section VII), except that Johnston used an approximation for $n\alpha$.

### A. Normand's Result

An equation resembling (17) was previously derived by Normand equation [(6) in [10]) from the physical assumptions under Case 2 in Section VII [23]. Apart from notation, the equations differ in that Normand's equation contains an additional parameter $C$, which was first introduced in an earlier paper [24]. Comparisons between model predictions and measured proton cross sections indicated that $C = 0.5$ is appropriate for some cases, while $C = 1$ is appropriate for some other cases [10]. This parameter $C$ is supported by physical arguments, and these arguments can be used to modify (17) as shown below.

The derivation of (17) started with one $\Omega$ function applicable to all ionization sources, but a different $\Omega$ for different sources may actually be appropriate, depending on whether the ionization produces high-density conditions (the carrier density liberated by the ionization greatly exceeds the doping density) or low-density conditions. For the high-density case, a low-order approximation for collected current at a reversed-biased depletion region boundary (DRB) is twice the minority carrier diffusion current, with the carrier-density gradient (used to calculate the diffusion current) calculated from the ambipolar diffusion equation [4], [5]. However, for low-density conditions at the DRB, the current is the minority carrier diffusion current instead of twice this current. Assuming that the high-density case applies to heavy ions, while proton reaction products create conditions ranging anywhere between low-density and high-density, the $\Omega$ appropriate for proton reactions is somewhere between 0.5 and 1 times the $\Omega$ appropriate for heavy ions. If $\Omega$ refers to heavy ions, then (2) should be modified by replacing $\Omega$ with $C\Omega$, where $C$ is some number between 0.5 and 1. Repeating the derivation of (17) while using the modified form of (2) gives

$$\sigma_{pr}(E) = T \int_0^\infty n\alpha \left( E,\, aL\frac{T}{C} \right) \frac{d\sigma_{hi}(L)}{dL}\, dL.$$

As long as $T$ is regarded as a fitting parameter, and not given a literal interpretation, the equation is just as convenient when expressed in terms of another fitting parameter $T' \equiv T/C$. In terms of $T'$, the equation becomes

$$\sigma_{pr}(E) = CT' \int_0^\infty n\alpha(E,\, aLT') \frac{d\sigma_{hi}(L)}{dL}\, dL$$

which conforms to Normand's result.

### B. Barak's Result

A result presented by Barak *et al.* ([25, eq. (6)], also in [26]) has the same form as (17). The two equations can be given a more similar appearance by changing variables from $L$ to $\varepsilon$ in (17), using $\varepsilon = LT$, and then integrating (17) by parts. However, a distinguishing characteristic of their work is that $n\alpha$ in (17) is replaced by an experimentally measured function (describing the spectra of charge liberated in surface barrier detectors via proton reactions) which is not subject to errors associated with the second physical postulate in Section II. Their $n\alpha$ is refined by including an implicit dependence on $T$. Unfortunately, this replacement for $n\alpha$ appears to be justified only for the conditions assumed under Case 2. Perhaps their work will inspire future work that will improve upon the second physical postulate while still retaining most of the generality allowed by the first physical postulate.

### C. Johnston's Result

An analysis by Johnston *et al.* [27] recognized that the collected charge relevant to heavy-ion induced SEL is a function of the lateral coordinates of the ion-hit location. This is consistent with Case 4, and an equation used by Johnston for calculating proton SEL cross sections can be reproduced by applying an approximation to (17). This approximation, which was used by Johnston, replaces a distributed spectrum of proton-induced reaction products with one predominant or representative type of reaction, in which the deposited energy is about 10 MeV (the liberated charge is about 0.46 pC, which is the number used by Johnston). The entire (i.e., includes all high-energy interactions) proton cross section is associated with this reaction, so $n\alpha$ is approximated by a step function given by

$$n\alpha(Q) = 2.5 \times 10^{-6}/\mu\text{m} \quad \text{if } Q \le 0.46 \text{ pC},$$
$$n\alpha(Q) = 0 \quad \text{if } Q > 0.46 \text{ pC}.$$

Substituting this step function for $n\alpha$ into (17) gives

$$\sigma_{pr} = \frac{T}{4 \times 10^5\ \mu\text{m}}\, \sigma_{hi} \left( \frac{44\ \mu\text{m}}{T}\, \frac{\text{MeV cm}^2}{\text{mg}} \right). \qquad (18)$$

When $n\alpha$ is a distributed spectrum, the heavy-ion cross section over a range of LET values contributes to $\sigma_{pr}$. The fact that $\sigma_{hi}$ is evaluated at only a single point in (18) is an artifact of the step-function fit used for $n\alpha$. The selected step function might be the best of the step-function fits for the intended application, because Johnston *et al.* [27] found good agreement between the measured and predicted $\sigma_{pr}$ for a number of cases representing a wide range of technologies. However, it is not yet clear whether this approach has limitations.

A distinguishing characteristic of their work is in the selection of a value for $T$. $T$ was taken to be the epi-layer thickness for the epitaxial devices, but the bulk devices require more thought. Computer simulations have shown that Case 4 does not apply to the bulk devices (of the cases considered in Section VII, Case 3 is the only possible candidate). Therefore, $T$ does not have a literal interpretation as assumed in Case 4, and some effective value is needed. From the point of view of Case 4, $T$ is a constant and is not necessarily the same as the charge-collection depth (which is a function of the lateral coordinates). The value that Johnston assigned to $T$ was the charge-collection depth calculated by computer simulations at the lateral center of a cylindrically symmetric device (the charge-collection depth is expected to be maximum at the lateral center). Johnston *et al.* provided a recipe instead of an equation, but the numerical entries in [27,

Table II]) can be reproduced by using (18) with $T$ obtained from [27, Fig. 5]).

### D. O'Neill's Results

O'Neill *et al.* provided two approaches for relating proton to heavy-ion cross sections. The first starts with a sophisticated technique [28] which calculates a spectrum of proton-induced liberated charge, which is a replacement for $n\alpha(Q)$ in (17) that is not subject to errors associated with the second physical postulate in Section II. Charge collection is assumed to be as described by the SV model, where the SV is an RPP. An effective LET associated with a proton reaction is calculated by dividing the liberated charge by the RPP thickness. Effective LET and liberated charge are equivalent descriptions, because one is proportional to the other. The proton-induced spectrum, plotted as a function of effective LET, is compared to a heavy-ion spectrum representing a space environment and plotted as a function of ion LET. The end result of this work is an upper bound for heavy-ion induced SEU rates derived from measured proton cross sections.

The applicability of this analysis may have some limitations (for reasons given below), but it might be possible to broaden the applicability by modifying the arguments. The proton-induced spectrum is plotted against effective LET while the heavy-ion spectrum is plotted against ion LET instead of effective LET. However, for hits at angles, there is also an effective LET for heavy-ions (also defined in terms of liberated charge divided by RPP thickness). A suggested modification to the authors' arguments includes the effects of angles as discussed below.

The basic idea is to compare the proton-induced spectrum to an *effective flux* describing heavy ions. An effective flux is a characteristic of both the environment and an assumed directional dependence describing device susceptibility to heavy ions. An effective flux for a given heavy-ion environment is different for devices having a nearly isotropic heavy-ion cross section (the RPPs are cubes) than for devices described by the cosine law (the RPP thickness is much smaller than the lateral dimensions). Effective flux can be rigorously defined for any model (RPP or other) in which there is a function $K$ satisfying

$$\sigma(L, \theta, \phi) = \int_0^\infty K(L', L, \theta, \phi) \frac{\partial \sigma_N(L')}{\partial L'} \, dL' \qquad (19)$$

where $\sigma(L, \theta, \phi)$ is the directional heavy-ion cross section evaluated at ion LET $L$ and in the direction described by the spherical-coordinate angles $\theta$ (measured from the device normal) and $\phi$, and $\sigma_N$ is the normal-incident heavy-ion cross section. The $\sigma_N$ here is the same as $\sigma_{hi}$ in (17), but the symbolism was changed to distinguish normal incidence from other directions. The function $K$ has a simple interpretation for devices described by Case 2 and with geometrically similar RPPs (i.e., each ratio of dimensions for one RPP equals the corresponding ratio for all other RPPs). For this case, $K(L', L, \theta, \phi)$ can be shown to be the normalized (by dividing by the area of the RPP face seen at normal incidence) directional cross section for an RPP having normal-incident threshold LET $L'$. $K(L', L, \theta, \phi)$ does not depend on the size of the RPP, but it does implicitly depend on the RPP dimension ratios, and explicitly depends on the threshold LET $L'$ of the RPP. The heavy-ion SEU rate $r_{hi}$ can be calculated from

$$r_{hi} = \int_0^\infty \int_{-1}^1 \int_0^{2\pi} h(L, \theta, \phi) \sigma(L, \theta, \phi) \, d\phi \, d(\cos\theta) \, dL$$

where $h$ is the differential (in LET) directional flux. Substituting (19) into the above equation gives

$$r_{hi} = \int_0^\infty H_{\text{eff}}(L') \frac{\partial}{\partial L'} \sigma_N(L') \, dL' \qquad (20)$$

where $H_{\text{eff}}$ is the integral effective flux defined by

$$H_{\text{eff}}(L') \equiv \int_0^\infty \int_{-1}^1 \int_0^{2\pi} h(L, \theta, \phi) K(L', L, \theta, \phi) \cdot d\phi \, d(\cos\theta) \, dL. \qquad (21)$$

From the interpretation of $K$ as a normalized directional cross section for an RPP, it is seen from (21) that $H_{\text{eff}}$ is the normalized SEU rate for the RPP. This makes effective flux associated with Case 2 very easy to calculate via a standard computer code that calculates heavy-ion SEU rates for RPPs. We calculate the SEU rate for the RPP, divide by the area of the face seen at normal incidence, and plot this normalized rate as a function of the threshold LET assigned to the RPP. The calculated effective flux will be independent of the thickness assigned to the RPP, as long as corresponding values are assigned to the critical charge (to be consistent with the selected threshold LET) and to the lateral dimensions (to be consistent with the selected dimension ratios).

Following O'Neill *et al.* [28], we now assume Case 2 conditions with all RPPs having the same thickness $T$. However, the $n\alpha(Q)$ in (17) is taken to be the spectrum calculated by the authors so that errors associated with the second physical postulate are removed. We next look for a constant $A$ satisfying

$$ATn\alpha(aLT) \geq H_{\text{eff}}(L) \quad \text{for all } L \qquad (22)$$

if it exists. If such an $A$ can be found, we can use (22) with (17) and (20) to obtain an upper bound on the heavy-ion rate given by

$$r_{hi} \leq A\sigma_{pr}. \qquad (23)$$

The result (23) is an extension of the authors' earlier work that accounts for directional effects when an $A$ satisfying (22) exists. If such an $A$ does not exist, we use an approach that is analogous to an approach used by the authors. This approach expresses the effective flux as a sum of two components constructed so that there is an $A$ associated with the flux component representing the majority of the heavy ions. A cruder but more generally applicable (not requiring an $A$) bound can be used for the smaller flux component because the accuracy requirement is more lenient for the smaller component.

One limitation still remains. This limitation is that the RPP model is required to be an adequate approximation, and the RPP dimensions must be known. This is because $H_{\text{eff}}$ and $n\alpha$ (the type of $n\alpha$ most suitable for this analysis) both depend on the RPP dimensions ($H_{\text{eff}}$ is strongly dependent on the dimension ratios, even if $n\alpha$ is not). This makes the values allowed for $A$

dependent on RPP dimensions. A second approach by the same authors [29] does not have this limitation.

The second approach also compares a proton-induced spectrum to a heavy-ion spectrum, but all spectra now refer to particle LET instead of effective LET, so comparisons are between the same types of spectra. If the two spectra are found to be proportional (for example), they should produce single event rates that are in the same proportion regardless of what model (RPP or other) applies; except for range effects. Ion range is important because charge collection depths can be quite large (sometimes 20 $\mu$m for SEL [27]), and the contributing depth is larger than the charge-collection depth, so ion range must sometimes be very large in order for initial LET to be an adequate characterization. The authors take range effects into consideration by distinguishing between different reaction products on the basis of range. One paper [29] distinguished reaction products having ranges less than 5 $\mu$m from the others. This is inadequate for the larger contributing depths, but more recent work extends the applicability to larger depths [30]. The theory in the present paper, which is most suitable for upper bound estimates of the proton cross section due to a conservative property of the second physical postulate, does not apply to this more recent work, so this work is not discussed further here.

### *E. The Petersen–Barak Equation*

Barak *et al.* [11] pointed out that empirical fits provided by Petersen [18] can be combined to give

$$\sigma_{pr} = 2.22 \times 10^{-5} \frac{\sigma_{hi,0}}{(L^{\#}_{0.25})^2} \tag{24}$$

where

- $\sigma_{hi,0}$ heavy-ion saturation cross section;
- $\sigma_{pr}$ (throughout this section) is the saturation cross section for protons;
- $L_{0.25}\#$ numerical part (when the units are MeV-cm$^2$/mg) of $L_{0.25}$ defined by $\sigma_{hi}(L_{0.25}) = 0.25 \times \sigma_{hi,0}$.

When Weibull parameters are given, $L_{0.25}$ can be calculated from

$$L_{0.25} = L_0 + (0.288)^{1/S} \times W.$$

This paper calls (24) the Petersen–Barak equation. This equation can be reproduced (approximately) by assuming that Case 1 applies and using (6) to write (12) as

$$\sigma_{pr} = \frac{Q_c}{a} A e^{-BQ_c} \int_0^\infty \frac{1}{L} \frac{d\sigma_{hi}(L)}{dL}\, dL \tag{25}$$

where the $E$ dependence was omitted from the notation because 200 MeV is assumed. Let $\tau_{0.25}$ be the charge-collection depth at the perimeter of the region represented by the cross section $\sigma_{hi}(L_{0.25})$. The critical LET for ion hits at this perimeter is $L_{0.25}$, so

$$Q_c = a\tau_{0.25}L_{0.25}$$

and (25) becomes

$$\sigma_{pr} = \tau_{0.25}L_{0.25} A e^{-aB\tau_{0.25}L_{0.25}} \int_0^\infty \frac{1}{L} \frac{d\sigma_{hi}(L)}{dL}\, dL. \tag{26}$$

To obtain the desired result, we use the *ad hoc* assumption

$$\tau_{0.25} = 3.38\ \mu\text{m}. \tag{27}$$

Using (27) and Table I with (26) gives

$$\sigma_{pr} = 6.76 \times 10^{-6} L_{0.25} e^{-0.349 L^{\#}_{0.25}} \int_0^\infty \frac{1}{L} \frac{d\sigma_{hi}(L)}{dL}\, dL. \tag{28}$$

When the $\sigma_{hi}$ curve is defined by a Weibull fit [as opposed to alternatives such as (7)], a fairly good approximation is

$$\int_0^\infty \frac{1}{L} \frac{d\sigma_{hi}(L)}{dL}\, dL \approx \frac{\sigma_{hi,0}}{L_{0.25}}. \tag{29}$$

Another approximation is

$$e^{-X} \approx \frac{0.4}{X^2} \text{ (within a factor of 1.4 when } 0.8 \le X \le 4.0). \tag{30}$$

The relevant values of $X$ in (30) depend on $L_{0.25}$. For many (not all) devices in Table II, the relevant $X$ results in (30) being accurate to within a factor of 1.4 (either too small or too large). Applying the approximations (29) and (30) to (28) produces the Petersen–Barak equation (24).

Because approximations were used to derive (24) from (28), we might expect (24) to be less accurate than (28). It turns out that (24) has a better track record than (28). The device data in Table II (excluding the SEL cases) were used to construct Table III. The ratio columns give $\sigma_{pr}$ calculated from the indicated equation divided by the measured $\sigma_{pr}$. Note that the ratio from (24) is usually closer to 1 than the ratio from (28). Other values for $\tau_{0.25}$ were tried with (28), but did not improve the track record for (28) when a common value for $\tau_{0.25}$ is assigned to all devices.

A suggested explanation as to why (24) fits the data better than (28) is that (28) assigns the same $\tau_{0.25}$ to all devices. Perhaps some other parameter is better than $\tau_{0.25}$ in the sense of being approximately the same for many devices. We could consider a common value for $Q_c$, instead of $\tau_{0.25}$, for all devices. A common $Q_c$ produces estimates that are a common multiple of the upper bounds in Table II. Selecting $Q_c$ to make the estimates equal to one-half the upper bounds will produce a moderately good track record, but still not as good as (24).

Assigning a common $\tau_{0.25}$ to all devices does not (at least not when Case 1 is assumed) fit the statistical trend as well as (24), and assigning a common $Q_c$ to all devices does not fit the statistical trend as well as (24). That (24) performs better than the above alternatives is not an accident, because (24) originated from empirical fits to extensive data sets. The property of being an empirical fit gives (24) an advantage and a disadvantage compared to a physics-based model. The disadvantage is that information sufficient to completely determine $\sigma_{pr}$ cannot be utilized by (24), even if such information were available. The advantage is that, when such information is not available (usually the case in practice), (24) has a high probability of producing an estimate that is nearly as good or better than a physics-based model containing *ad hoc* values for the unknown parameters.

TABLE III
THE RATIO COLUMNS GIVE $\sigma_{pr}$ CALCULATED FROM THE INDICATED EQUATION (USING DATA IN Table II) DIVIDED BY THE MEASURED $\sigma_{pr}$. NOTE THAT THE PETERSEN–BARAK EQUATION (24) PERFORMS BETTER (THE RATIO IS CLOSER TO 1) THAN (28) FOR THE MOST OF THE CASES LISTED

| Part | Ratio from (24) | Ratio from (28) |
|---|---|---|
| SMJ44100 | 1.39 | 1.60 |
| 62256R | 0.796 | 0.578 |
| IBM 16MEG | 0.613 | 0.213 |
| MT4C1004C | 1.24 | 1.31 |
| KM41C4000Z-8 | 1.06 | 0.969 |
| 01G9274 | 1.20 | 0.106 |
| OW 62256 | 0.776 | 0.469 |
| MT4C4001 | 2.09 | 2.40 |
| HM6116 | 0.394 | 0.375 |
| 62832H | 0.522 | 0.293 |
| 2901B | 1.07 | 0.999 |
| TC514100Z-10 | 0.963 | 1.16 |
| HM 65656 | 1.50 | 1.72 |
| MB814100 10PSZ | 2.03 | 2.36 |
| HYB514100J-10 | 1.10 | 1.35 |
| LUNA C | 1.01 | 0.599 |
| D424100V-80 | 1.17 | 1.22 |
| HM6516 | 1.80 | 1.01 |
| Fairchild 93L422 (bipolar) | 2.26 | 0.542 |
| Samsung 16M 3.3V DRAM | 0.779 | 0.789 |
| Hitachi 16M 3.3V DRAM | 0.785 | 0.976 |
| Micron 16M 3.3V DRAM | 1.05 | 1.30 |
| IBM E 16M 3.3V DRAM | 0.971 | 1.17 |

## IX. CONCLUSIONS

A common situation is that in which a device has been tested with heavy ions for SEU and/or SEL, but not yet tested with protons. A proton test is an additional expense, so there is a motivation to use heavy-ion data to predict proton cross sections. Of the results derived here, the upper bound estimate is the most useful in terms of practical applications, because it is derived from the most generic assumptions and does not require information that is not available. A disadvantage is that this estimate is sometimes excessively conservative (pessimistic). The method was used to estimate SEU rates in a proton environment for numerous devices of interest to a JPL flight project. An additional (but not excessive) conservatism was included by assigning the 200 MeV cross section to all protons having energies greater than 7 MeV. The observation from this application is that the rate estimates are often acceptable to a flight project, even though the estimates might be excessively conservative, in which case a proton test is not needed. If the estimate predicts problems for a flight project, a proton test is needed to obtain a smaller estimate, but the upper bound does at least reduce the number of tests that are required.

Practical applications of the results intended to accurately estimate the proton cross section (instead of a bound for it) are more limited, because additional information is required. It must first be known which model (e.g., one of the cases in Section VII) is the best choice, and then model parameters must be estimated. If it is (somehow) known that Case 1 is an adequate approximation, an estimate is needed for the critical charge. If it is (somehow) known that either Case 2 or Case 4 is an adequate approximation, an estimate is needed for the RPP thickness or the contributing depth. If it is (somehow) known that the latter cases are inappropriate, but the more versatile Case 3 is an adequate approximation, an estimate is needed for the function $g(z)$. Future work might find inexpensive methods for obtaining the required information, but another reason for presenting these results is academic curiosity. It is interesting to see the similarities and differences between various models, including models previously presented by others.

An empirical fit applicable to SEU (not SEL), which this paper calls the Petersen–Barak equation, was also discussed. This is not only one of the simplest results, but also has a high probability of producing an estimate for the saturation proton cross section that is nearly as good or better than a physics-based model containing ad hoc values for unknown parameters. If the information that is needed to take full advantage of a physics-based model is not available (usually the case), and if the objective is to obtain a "most probable estimate," as opposed to an upper bound, this equation should be considered.

## APPENDIX
## DERIVATION OF EQUATIONS (3) AND (16)

Let the coordinate system be oriented so that the $z$ axis is parallel to the heavy-ion trajectory. The device orientation relative to this coordinate system is arbitrary. For a normal-incident orientation, $\sigma_{hi}$ is the normal-incident heavy-ion cross section. Otherwise, $\sigma_{hi}$ is a directional cross section. The location of an ion trajectory is given by two coordinates $x$ and $y$. Let $Q(x, y)$ be the collected charge produced by an ion with LET $L$ and having a trajectory at $x, y$. Using the selected device orientation to define the charge-collection efficiency function $\Omega(x, y, z)$, we have

$$Q(x, y) = aL \int_{-\infty}^{\infty} \Omega(x, y, z)\, dz. \tag{A1}$$

We are calling $Q$ the collected charge for conceptual clarity, although it could be some other quantity. If so, then (A1) is taken to be the definition of $Q$, with $\Omega$ defined in the first physical postulate. The first physical postulate implies that $\sigma_{hi}(L)$ is the area of the set of points $(x, y)$ in the plane satisfying

$$Q(x, y) > Q_c.$$

This set of points is the same as the set satisfying

$$\tau(x, y) > \frac{Q_c}{aL}$$

where $\tau$ is the normalized collected charge (also called the charge-collection depth) defined by

$$\tau(x, y) \equiv \frac{Q(x, y)}{aL} = \int_{-\infty}^{\infty} \Omega(x, y, z)\, dz. \tag{A2}$$

Therefore

$$\sigma_{hi}(L) = F\left(\frac{Q_c}{aL}\right) \tag{A3}$$

where $F$ is defined by

$$F(v) \equiv \text{area of the set of points } (x, y) \text{ satisfying } \tau(x, y) > v,$$

i.e., $F(v)$ is the cross section for the normalized charge to exceed $v$.

A mathematical theorem can be derived after defining some additional symbolism. Let $s$ be any set of points in the $x$, $y$ plane having a defined area. The area of $s$ is denoted $A[s]$, and the compliment of $s$ (all points in the plane not in $s$) is denoted $s^*$. For any $v \geq 0$, define

$$S(v) \equiv \text{the set of points } (x, y) \text{ satisfying } \tau(x, y) > v.$$

Now select a positive number $\Delta v$ and let $v_n \equiv n\Delta v\,(n = 0, 1, 2, \cdots)$. Define each of the sets $S_1, S_2, \cdots$, by

$$S_n \equiv \text{the set of points } (x, y) \text{ satisfying } v_n \geq \tau(x, y) > v_{n-1} \qquad (n = 1, 2, \cdots).$$

Some of the above sets may be empty but this does not invalidate the theory. The $x$, $y$ plane is the union of $S(0)$ with $S^*(0)$, while $S(0)$ is the union of the sets $S_1, S_2, \cdots$. Therefore an arbitrary set $s$ can be expressed as

$$s = [s \cap S^*(0)] \cup [\cup_n \{s \cap S_n\}].$$

The right side is a union of nonintersecting sets, so

$$\int_s G(\tau(x, y))\,dx\,dy = \int_{s \cap S^*(0)} G(\tau(x, y))\,dx\,dy + \sum_{n=1}^{\infty} \int_{s \cap Sn} G(\tau(x, y))\,dx\,dy$$

for any function $G$ such that the integral on the left side exists. Using the definition of $S_n$ and the fact that $\tau = 0$ on $S^*(0)$ gives

$$\int_s G(\tau(x, y))\,dx\,dy = G(0)A[s \cap S^*(0)] + \sum_{n=1}^{\infty} G(v_n)A[s \cap S_n] \quad \text{(A4)}$$

which is valid to first order in $\Delta v$ (we will later take the limit as $\Delta v \to 0$). The definitions of the sets imply that

$$S(v_{n-1}) = S(v_n) \cup S_n$$

so

$$s \cap S(v_{n-1}) = [s \cap S(v_n)] \cup [s \cap S_n].$$

The right side is a union of nonintersecting sets, so

$$A[s \cap S(v_{n-1})] = A[s \cap S(v_n)] + A[s \cap S_n].$$

This equation allows us to write (A4) as

$$\int_s G(\tau(x, y))\,dx\,dy = G(0)A[s \cap S^*(0)] - \sum_{n=1}^{\infty} G(v_n) \cdot \frac{A[s \cap S(v_n)] - A[s \cap S(v_n - \Delta v)]}{\Delta v}\,\Delta v.$$

Taking the limit as $\Delta v \to 0$ gives

$$\int_s G(\tau(x, y))\,dx\,dy = G(0)A[s \cap S^*(0)] - \int_0^{\infty} G(v)\frac{dA[s \cap S(v)]}{dv}\,dv$$

for any point set $s$ and any function $G$ such that the integrals exist. In particular, if $G(0) = 0$, we can let $s$ be the entire $x$, $y$ plane to get

$$\int G(\tau(x, y))\,dx\,dy = -\int_0^{\infty} G(v)\frac{dF(v)}{dv}\,dv \quad \text{if } G(0) = 0$$

where the integral on the left integrates over the entire $x$, $y$ plane, and we used $A[s \cap S(v)] = A[S(v)] = F(v)$. The above equation can be expressed in terms of $\sigma_{hi}$ by using (A3) and changing variables in the integral on the right to get

$$\int G(\tau(x, y))\,dx\,dy = \int_0^{\infty} G\left(\frac{Q_c}{aL}\right)\frac{d\sigma_{hi}(L)}{dL}\,dL \quad \text{if } G(0) = 0. \quad \text{(A5)}$$

This equation is used to derive (16) in the main text. To derive (3), we apply (A5) to the special case given by $G(\xi) = \xi$. The integral on the left becomes the integral of $\tau(x, y)$ on the $x$, $y$ plane, which, according to (A2), is the volume integral of $\Omega$. The result is

$$\int \Omega(x, y, z)\,dx\,dy\,dz = \frac{Q_c}{a}\int_0^{\infty} \frac{1}{L}\frac{d\sigma_{hi}(L)}{dL}\,dL. \quad \text{(A6)}$$

Note that a change in the device orientation will rotate the function $\Omega$, but this does not change the volume integral on the left side of (A6). This implies that the right side has the same value whether $\sigma_{hi}$ is the normal-incident cross section or the directional cross section for some other direction.

## REFERENCES


[1] E. L. Petersen, "Approaches to proton single-event rate calculations," *IEEE Trans. Nucl. Sci.*, vol. 43, pp. 496–504, Apr. 1996.

[2] J. M. Bisgrove, J. E. Lynch, P. J. McNulty, W. G. Abdel-Kader, V. Kletnieks, and W. A. Kolasinski, "Comparison of soft errors induced by heavy ions and protons," *IEEE Trans. Nucl. Sci.*, vol. NS-33, pp. 1571–1576, Dec. 1986.

[3] L. Edmonds, "A graphical method for estimating charge collected by diffusion from an ion track," *IEEE Trans. Nucl. Sci.*, vol. 43, pp. 2346–2357, Aug. 1996.

[4] ——, "Charge collection from ion tracks in simple EPI diodes," *IEEE Trans. Nucl. Sci.*, vol. 44, pp. 1448–1463, June 1997.

[5] ——, "Electric currents through ion tracks in silicon devices," *IEEE Trans. Nucl. Sci.*, vol. 45, pp. 3153–3164, Dec. 1998.

[6] E. L. Petersen, "Interpretation of heavy ion cross section measurements," *IEEE Trans. Nucl. Sci.*, vol. 43, pp. 952–959, June 1996.

[7] J. Barak, J. Levinson, A. Akkerman, E. Adler, A. Zentner, D. David, Y. Lifshitz, M. Hass, B. E. Fischer, M. Schlogl, M. Victoria, and W. Hajdas, "Scaling of SEU mapping and cross section, and proton induced SEU at reduced supply voltage," *IEEE Trans. Nucl. Sci.*, vol. 46, pp. 1342–1353, Dec. 1999.

[8] E. L. Petersen, "Cross section measurements and upset rate calculations," *IEEE Trans. Nucl. Sci.*, vol. 43, no. 6, pp. 2805–2813, Dec. 1996.

[9] L. W. Massengill, M. L. Alles, S. E. Kerns, and K. L. Jones, "Effects of process parameter distributions and ion strike locations on SEU cross-section data," *IEEE Trans. Nucl. Sci.*, vol. 40, pp. 1804–1811, Dec. 1993.

[10] E. Normand, "Extensions of the burst generation rate method for wider application to proton/neutron-induced single event effects," *IEEE Trans. Nucl. Sci.*, vol. 45, pp. 2904–2914, Dec. 1998.

[11] J. Barak, R. A. Reed, and K. A. LaBel, "On the figure of merit model for SEU rate calculations," *IEEE Trans. Nucl. Sci.*, vol. 46, pp. 1504–1510, Dec. 1999.
[12] M. B. Chadwick and E. Normand, "Use of new ENDF/B-VI proton and neutron cross sections for single event upset calculations," *IEEE Trans. Nucl. Sci.*, vol. 46, pp. 1386–1394, Dec. 1999.
[13] L. Edmonds, "SEU cross sections derived from a diffusion analysis," *IEEE Trans. Nucl. Sci.*, vol. 43, no. 6, pp. 3207–3217, Dec. 1996.
[14] J. Levinson, A. Akkerman, M. Victoria, M. Hass, D. Ilberg, M. Alurralde, R. Henneck, and Y. Lifshitz, "New insight into proton-induced latchup: Experiment and modeling," *Appl. Phys. Lett.*, vol. 63, no. 21, pp. 2952–2954, Nov. 1993.
[15] E. L. Petersen, J. C. Pickel, J. H. Adams Jr, and E. C. Smith, "Rate prediction for single event effects—A critique," *IEEE Trans. Nucl. Sci.*, vol. 39, pp. 1577–1599, Dec. 1992.
[16] E. L. Petersen, "The relationship of proton and heavy ion upset thresholds," *IEEE Trans. Nucl. Sci.*, vol. 39, no. 6, pp. 1600–1604, Dec. 1992.
[17] P. Calvel, C. Barillot, P. Lamothe, R. Ecoffet, S. Duzellier, and D. Falguere, "An empirical model for predicting proton induced upset," *IEEE Trans. Nucl. Sci.*, vol. 43, pp. 2827–2832, Dec. 1996.
[18] E. L. Petersen, "The SEU figure of merit and proton upset rate calculations," *IEEE Trans. Nucl. Sci.*, vol. 45, pp. 2550–2562, Dec. 1998.
[19] D. K. Nichols, M. A. Huebner, W. E. Price, L. S. Smith, and J. R. Coss, *Heavy Ion Induced Single Event Phenomena (SEP) Data for Semiconductor Devices from Engineering Testing*: Jet Propulsion Laboratory Publication 88-17, July 1988.
[20] D. K. Nichols, W. E. Price, and J. L. Andrews, "The dependence of single event upset on proton energy (15-590 MeV)," *IEEE Trans. Nucl. Sci.*, vol. NS-, pp. 2081–2084, Dec. 1982.
[21] J. B. Langworthy, "Depletion region geometry analysis applied to single event sensitivity," *IEEE Trans. Nucl. Sci.*, vol. 36, pp. 2427–2434, Dec. 1989.
[22] E. L. Petersen, J. C. Pickel, E. C. Smith, P. J. Rudeck, and J. R. Letaw, "Geometrical factors in SEE rate calculations," *IEEE Trans. Nucl. Sci.*, vol. 40, pp. 1888–1909, Dec. 1993.
[23] E. Normand and T. J. Baker, "Altitude and latitude variations in avionics SEU and atmospheric neutron flux," *IEEE Trans. Nucl. Sci.*, vol. 40, pp. 1484–1490, Dec. 1993.
[24] A. Taber and E. Normand, "Single event upset in avionics," *IEEE Trans. Nucl. Sci.*, vol. 40, pp. 120–126, Apr. 1993.
[25] J. Barak, J. Levinson, A. Akkerman, Y. Lifshitz, and M. Victoria, "A simple model for calculating proton induced SEU," in *Proc. RADECS'95*, Arcachon, France, Sept. 18–22, 1995, pp. 431–436.
[26] ——, "A simple model for calculating proton induced SEU," *IEEE Trans. Nucl. Sci.*, vol. 43, pp. 979–984, June 1996.
[27] A. Johnston, G. Swift, and L. Edmonds, "Latchup in integrated circuits from energetic protons," *IEEE Trans. Nucl. Sci.*, vol. 44, pp. 2367–2377, Dec. 1997.
[28] P. O'Neill, G. Badhwar, and W. Culpepper, "Risk assessment for heavy ions of parts tested with protons," *IEEE Trans. Nucl. Sci.*, vol. 44, pp. 2311–2314, Dec. 1997.
[29] ——, "Internuclear cascade-evaporation model for LET spectra of 200 MeV protons," *IEEE Trans. Nucl. Sci.*, vol. 45, pp. 2467–2474, Dec. 1998.
[30] P. O'Neill, presented at the 12th Single Events Effects Symp., Manhattan Beach, CA, Apr. 11–13, 2000.